In: Mang, H. A., Rammerstorfer, F. G. &
Eberhardsteiner, J. (eds.). Proceedings of the 5th World
Congress on Computational Mechanics. Vienna, Austria,
7–12 July, 2002. Vienna: Vienna University of Technology,
2002. 10 p. Available: http://wccm.tuwien.ac.at.

Electromechanical Interaction in Rotor Vibrations of Electric Machines

Timo P. Holopainen*

VTT Industrial Systems
Technical Research Centre of Finland, P.O. Box 1705, FIN-02044 VTT, Finland
e-mail: timo.holopainen@vtt.fi

Asmo Tenhunen and Antero Arkkio

Laboratory of Electromechanics
Helsinki University of Technology, P.O. Box 3000, FIN-02015 HUT, Finland
e-mail: asmo.tenhunen@hut.fi, antero.arkkio@hut.fi

Key words: Rotors, vibration analysis, electromechanical interaction, electric machines, finite element analysis

Abstract
In electric machines the electromagnetic fields interact with the deformations of machine structures. At low frequencies the electromagnetic system may couple distinctly with the mechanical one. This electromechanical interaction changes the vibration characteristics of the machine; e.g., it may induce additional damping or cause rotordynamic instability. To study these interaction effects, an electromechanical simulation model for the rotor vibrations of electric machines was developed. A time-stepping, finite element analysis was used for the solution of these system equations. The complete system is non-linear due to the saturation of magnetic materials. In addition, a spatially linearized version of the complete simulation model was developed. In this model, the effects of non-linear saturation can be calculated before the actual simulation. The developed simulation models were applied to study the vibration characteristics of a modified 15 kW electric motor. The impulse excitation exerted on the rotor was used as the loading for the transient analyses. The rotordynamic stability was illustrated by plotting the orbits of the rotor with two separate shaft stiffness. In addition, the response signals and frequency response functions obtained by the simulation models were compared. The complete and linearized models yielded almost similar results. These numerical results indicate that the linearized simulation model can be used as a good approximation for the electromechanical interaction in rotor vibrations of electric machines. Moreover, the linearized model is numerically very effective compared to the complete simulation model.

1 Introduction

An electric motor converts electric energy to mechanical one. The magnetic field in the air gap of the machine generates the tangential forces required for the torque generation. In addition, the field produces other force components that interact with the machine structures and may cause harmful vibrations. At relatively low frequencies, the vibration amplitudes may be large enough to couple the electromagnetic system with the mechanical one. This electromechanical interaction changes the vibration characteristics of the machine; e.g., it may induce additional damping or cause rotordynamic instability.

Früchtenicht, Jordan and Seinsch [1] developed an analytic model for the electromechanical forces between the rotor and stator, when the rotor is in circular whirling motion. Using this model, and assuming synchronous whirling motion, they determined the stiffness and damping coefficients induced by the electromagnetic field. They used these coefficients in a simple mechanical rotor model and studied the effects of electromechanical interaction. Using this model, and carefully designed experimental arrangements, they found out that the electromechanical interaction can cause rotordynamic instability. Later on, Belmans, Vandenput and Geysen [2] studied both analytically and experimentally induction motors operating on supercritical speed range. Their calculation model resembled to that of Früchtenicht et al. [1], but they focused on two-pole machines. They concluded that one potential reason for the rotordynamic instability results from the electromagnetic damping coefficient which may be negative. Skubov and Shumakovich [3] developed an analytic electromechancial model and studied the rotordynamic instability. They found out that the tangential component of the electromagnetic total force may be the reason for the instability.

Arkkio et al. [4] presented a simple parametric model for the electromagnetic forces acting between the rotor and stator when the rotor is in whirling motion. They determined the model parameters of an electric motor by numerical simulations including the non-linear saturation of magnetic materials. In addition, Arkkio et al. validated the numerical results by extensive measurements. Holopainen, Tenhunen and Arkkio [5] connected this parametric force model with a simple mechanical rotor model. Using this simple model they studied the effects of electromechanical interaction on vibration characteristics and particularly on rotordynamic instability. This simple electromechanical model is numerically very effective, because the non-linear analysis of electromagnetic fields can be carried out before the electromagnetic and mechanical systems are coupled together. This means, that the model is linearized around the equilibrium point in the actual operation conditions. However, there is an open question, whether this approach is feasible. The aim of this study was to validate this simple electromechanical model against a more advanced, in one way complete, simulation model, in which the electromagnetic field equations and the mechanical equations of motion are solved simultaneously.

2 Methods of analysis

2.1 Complete simulation model

The simulation of the electromechanical system was based on the time-stepping, finite-element analysis. The details of the calculation of the magnetic field are presented by Arkkio [6]. The magnetic field in the core region of the motor was assumed to be two-dimensional. End-winding impedances were used in circuit equations of the windings to model approximately the end effects. Second-order, isoparametric, triangular elements were used for the electromagnetic fields. A typical finite element mesh for the cross section of the test motor contained about 10 000 nodes.

To model the mechanical behavior of the system, we applied the Jeffcott rotor model. The rotor core was modeled as a rigid cylinder located at the middle of a uniform, massless, flexible shaft. The shaft was simply supported at its ends by the rigid frictionless bearings. The damping forces were neglected in order to emphasize the effects of electromagnetic forces, and the cylinder was assumed to move only in transversal plane, or more precisely in *xy*-plane. The origin of this plane was assumed to coincide with the rotation axis, and the center position of the rotor core was defined by a complex variable

$$z(t) = x(t) + \mathrm{i}\, y(t) . \tag{1}$$

The equation of motion of this simple rotor, using the complex co-ordinates approach, can be written

$$m\ddot{z} + kz = f(t), \tag{2}$$

where m is the mass of the disc, k is the shaft stiffness coefficient, and f is the excitation force.

The electromechanical interaction was modeled by moving the center point of the electromagnetic rotor model, which was rotated at the mechanical angular frequency, according to the motion of the mechanical rotor model. Likewise, the electromagnetic total force exerted on the rotor was fed back to the mechanical rotor model. The stator was mechanically modeled as a rigid body. Changing the finite-element mesh in the air gap enabled the relative motion between the rotor and stator. The method presented by Coulomb [7] was used for computing the electromagnetic forces. It is based on the principle of virtual work, and the force is obtained as a volume integral computed in an air layer surrounding the rotor. In the two-dimensional formulation, the calculation reduces to a surface integration over the finite elements in the air gap.

The magnetic field and circuit equations were discretized and solved together with the mechanical system. The time-dependence of the variables was modeled by the Crank-Nicholson method. The magnetic field, the currents, and the rotor motion were obtained directly in the solution of the equations.

Several simplifications have been made in order to keep the amount of computation on a reasonable level. The magnetic field in the core of the machine is assumed to be two-dimensional. The laminated iron core is treated as a non-conducting, magnetically non-linear medium, and the non-linearity is modeled by a single valued magnetization curve. The unipolar flux that may be associated with eccentricity is neglected. However, the method of analysis should model properly the effects of the equalizing currents, non-skewed slotting and saturation.

2.2 Linearized simulation model

Arkkio et al. [4] presented a low order linear model for the electromagnetic forces between the rotor and stator. The proposed transfer function model can be written in complex form as

$$F_{em}(s) = K(s) z(s) , \tag{3}$$

where F_{em} is the complex valued electromagnetic force exerted on the rotor, z is the complex valued displacement of the rotor center, s is Laplace variable, and $K(s)$ is a second order transfer function

$$K(s) = k_0 + \frac{k_{p-1}}{s - a_{p-1}} + \frac{k_{p+1}}{s - a_{p+1}} , \tag{4}$$

where k_0, k_{p-1}, k_{p+1}, a_{p-1}, and a_{p+1} are the parameters of the model, and p refers to the number of pole pairs of the machine. The subscripts of the parameters, $p-1$ and $p+1$, refer to the respective eccentricity harmonics of the electromagnetic fields. The parameters $k_{p\pm1}$ and $a_{p\pm1}$ are generally complex valued.

Arkkio et al. [4] determined the force parameters of an electric motor by calculating the electromagnetic forces induced by circular whirling motion ($s = \mathrm{i}\omega$). Figure 1 shows the radial and tangential force components as a function of whirling frequency. The 15 kW four-pole cage induction motor, which is also the test motor of our study, is rotated at the rated speed and supplied by the rated voltage. The whirling radius is 11 % of the radial air-gap length. The radial component is defined in the direction of the shortest air gap and the tangential component perpendicular to the radial one.

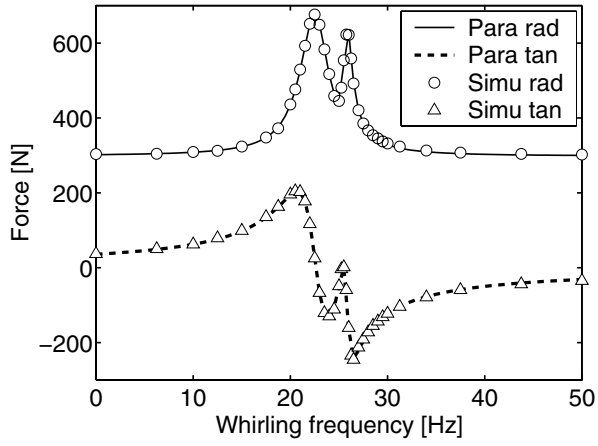

Figure 1: The radial and tangential forces as function of the whirling frequency. The discrete points represent the simulation results and the continuous curves are obtained by a curve fitting procedure together with the parametric model [4].

The linear second order transfer function of Equation (4) correspond to the equations

$$\begin{aligned} \dot{q}_{p-1} &= a_{p-1} q_{p-1} + k_{p-1} z(t) \\ \dot{q}_{p+1} &= a_{p+1} q_{p+1} + k_{p+1} z(t) \\ F_{em}(t) &= q_{p-1} + q_{p+1} + k_0 z(t) \end{aligned} \tag{5}$$

where q_{p-1} and q_{p+1} are new variables related to the eccentricity harmonics $p-1$ and $p+1$ of the air-gap field.

The linearized electromechanical rotor equations were obtained by combining the mechanical equations of motion (2) with the equations of electromagnetic forces (5). Thus, the coupled system of equations can be written

$$\begin{aligned} m\ddot{z} + (k - k_0) z - q_{p-1} - q_{p+1} &= f(t) \\ \dot{q}_{p-1} &= a_{p-1} q_{p-1} + k_{p-1} z \\ \dot{q}_{p+1} &= a_{p+1} q_{p+1} + k_{p+1} z \end{aligned} \tag{6}$$

These are the differential equations of the linearized simulation model used later in the numerical examples.

3 Simulation results

3.1 The studied motor

The studied motor was a 15 kW four-pole cage induction motor. The main parameters of the motor are given in Table 1, and the cross-sectional geometry is shown in Figure 2. The effective stiffness and mass of the rotor were roughly estimated. The mechanical damping was neglected. Arkkio et al. [4] used this motor as an example for extensive numerical simulations of electromagnetic forces in forced circular whirling motion. They verified the calculation results by measurements. Table 2 shows the electromagnetic force parameters determined in that investigation and employed in this study in the linearized simulation model.

Table 1: Parameters of the 15 kW induction motor.

Parameter	Value
Nominal shaft stiffness [N/m]	$1.5\cdot10^8$
Mass of the rotor [kg]	30
Number of poles	4
Number of phases	3
Number of parallel paths	1
Outer diameter of the stator core [mm]	235
Core length [mm]	195
Air-gap diameter [mm]	145
Radial air-gap length [mm]	0.45
Number of stator slots	36
Number of rotor slots	34
Skew of rotor slots	0
Connection	Delta
Rated voltage [V]	380
Rated frequency [Hz]	50
Rated current [A]	28
Rated power [kW]	15

Table 2: The electromagnetic force parameters of the 15 kW induction motor. The meaning of the parameters is presented in Equations (3) and (4).

Parameter	Value	Unit
k_0	$6.22\cdot10^6$	N/m
k_{p-1}	$(17.5+\mathrm{i}\,6.82)\cdot10^6$	N-rad/m-s
k_{p+1}	$(87.9+\mathrm{i}\,8.65)\cdot10^6$	N-rad/m-s
a_{p-1}	$2\pi(-0.54+\mathrm{i}\,25.8)$	rad/s
a_{p+1}	$2\pi(-1.80+\mathrm{i}\,22.6)$	rad/s

We studied the motor operating at its rated power (15 kW), supplied by the rated voltage (380 V), and the rotor was running at the rated slip (0.032). In the simulations, lower than the nominal values for the shaft stiffness were used in order to underline the effects of electromechanical interaction. A similar approach was employed by Früchtenicht et al. [1] and Belmans et al. [2].

3.2 Electromagnetic field in whirling motion

The magnetic field, producing forces between the rotor and stator, is required to convert the electric energy into the mechanical form. If the rotor is concentric with the stator, the total force between the rotor and stator is zero. If the rotor is moved from the center point, the magnetic field of an ideal motor is disturbed. To illustrate this phenomenon, we compared the magnetic fields of the studied motor in two conditions. Either the center point of the rotor was forced to move along a circular path at a constant whirling speed, which was the same as the rotation speed of the rotor, i.e. $24.25\,\mathrm{Hz}$, or the center point of the rotor was hold fixed in the center. The motor was simulated in rated operation conditions with the exception of slip, which was 0.03. A relatively long simulation time, $t = 2.6\,\mathrm{s}$, was required in order to eliminate the effects of initial transients and to distinguish the disturbed field induced by the whirling motion. Figure 2 shows the electromagnetic field in studied motor with whirling rotor, and the difference of the above mentioned two fields, at time $t = 2.6\,\mathrm{s}$. At that instant of time, the angular position of the shortest air gap due to the whirling motion is 18.0 degrees in respect to the horizontal line. Further, the amplitude of the total electromagnetic force vector, exerted on the rotor, was 696 N, and the angle –4.6 degrees in respect to the horizontal line.

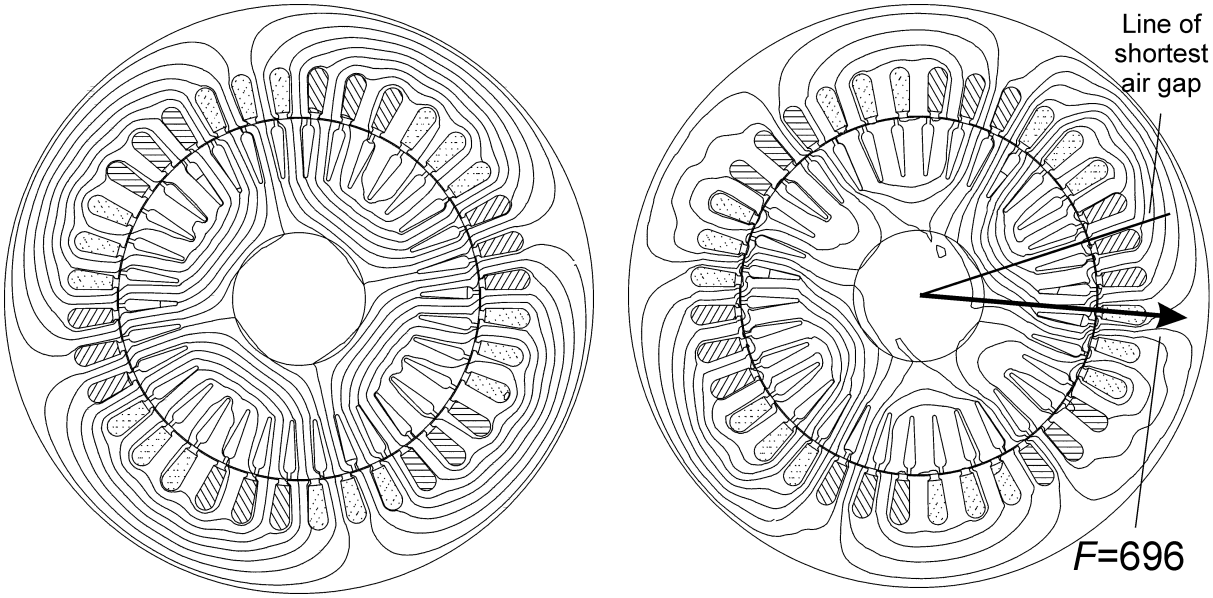

Figure 2: On the left is the magnetic field of the motor obtained by the whirling rotor with radius $50\ \mu\mathrm{m}$, i.e., about 11 % of the air gap length. The flux between any two curves is $4.25\,\mathrm{mWb/m}$. On the right is the difference of the magnetic fields obtained by the whirling rotor and by the fixed concentric rotor. In this case the flux between any two curves is $0.093\,\mathrm{mWb/m}$.

3.2.1 Orbital motion of rotor

The electromechanical interaction may induce rotordynamic instability [1, 2], e.g., by supplying electric energy via circulatory forces into the mechanical energy of transversal vibration [5]. We

studied the rotordynamic stability by simulating the motor with two separate shaft stiffness. A rectangular pulse in horizontal direction excited the rotor. The excitation force was 30 N, the length of the pulse 0.01 s, and thus, the first cut-off frequency 100 Hz. Figure 3 shows the orbits of the rotor center obtained by the complete simulation model. The simulation time was 1.0 s. The convergent spiral represents the stable rotordynamic behavior and the opening spiral the unstable behavior. The stability limit for the shaft stiffness obtained by the linearized model is $k = 1.4 \cdot 10^7$ N/m .

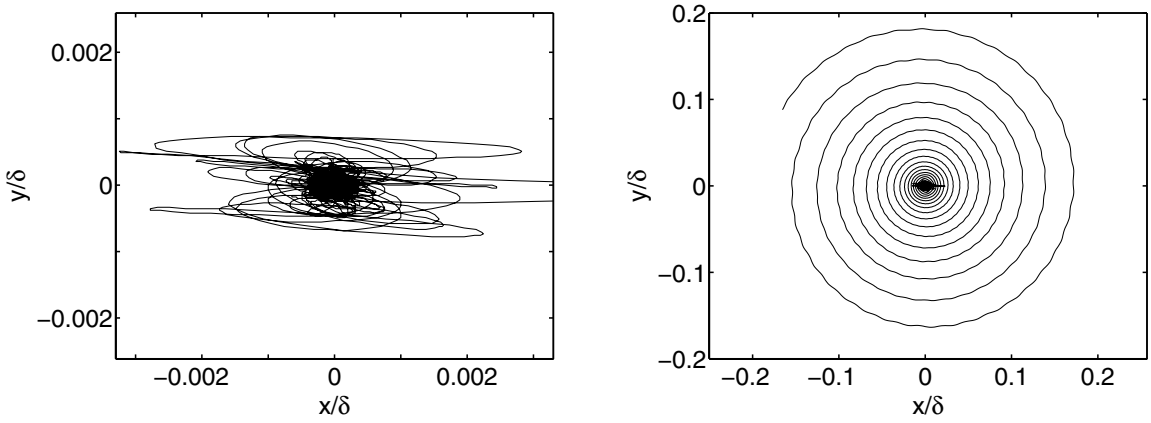

Figure 3: The orbit of rotor center obtained by the complete simulation model with the shaft stiffness $k = 1.6 \cdot 10^7$ N/m (on the left) and $k = 1.2 \cdot 10^7$ N/m (on the right). The displacements are related to the air gap length, $\delta = 0.45$ mm .

3.2.2 Transient response

One way to compare the complete and linearized simulation models is to plot the response signals induced by the same excitation at equivalent operation conditions. Figure 4 shows the horizontal and vertical displacement signals for the horizontal impulse excitation. In the simulations, the shaft stiffness $k = 1.3 \cdot 10^7$ N/m was used yielding the first flexural frequency 105 Hz without the effects of electromagnetic forces, and 78 Hz with the electromechanical interaction. The results obtained by the complete and linearized simulation models are shown.

3.2.3 Frequency response functions

Another, more comprehensive, way to study the similarity of the two system models is to compare the frequency responses. Figure 5 shows the frequency response plots between the horizontal and vertical displacements and the horizontal excitation. The shaft stiffness $k = 1.4 \cdot 10^7$ N/m was applied yielding the first flexural frequency 109 Hz without the effects of electromagnetic forces. The length of the horizontal excitation pulse was 0.01 s and the force amplitude 30 N. The first cut-off frequency of this excitation is 100 Hz. The total simulation time was two seconds. In the complete simulation analysis the time step was chosen to be $\Delta t = 0.05$ ms . Every sixth calculation point was used later in the spectral analysis. Thus, the sampling time for the spectral analysis was $\Delta t = 0.3$ ms . The exponential window ($e^{-\alpha t}$, $\alpha = 1$ rad/s) was applied to reduce the discontinuity at the end of the simulated data, and thus, to avoid the effects of leakage. Leakage is a direct consequence of the finite sample length coupled with the assumption of periodicity [8]. To increase the spectral resolution, the sample size was

extended to be 4.9149 s by adding zeros in the end of the simulated time data. Thus, in the discrete Fourier transform the number of points was 2^{14} (= 16384). The simulation procedure with the linearized model was mainly similar. However, the explicit Runge-Kutta solver was used with the maximum time step $\Delta t_{\max} = 1\,\text{ms}$ [9]. The total simulation time was 4.9149 s, but the zero padding technique was not applied. The discrete response values in the predefined sampling points ($n = 2^{14}$, $\Delta t = 0.3\,\text{ms}$) were obtained by the cubic spline interpolation. Thus, the main difference between the complete and the linearized simulation approaches was the modeling of the electromechanical interaction.

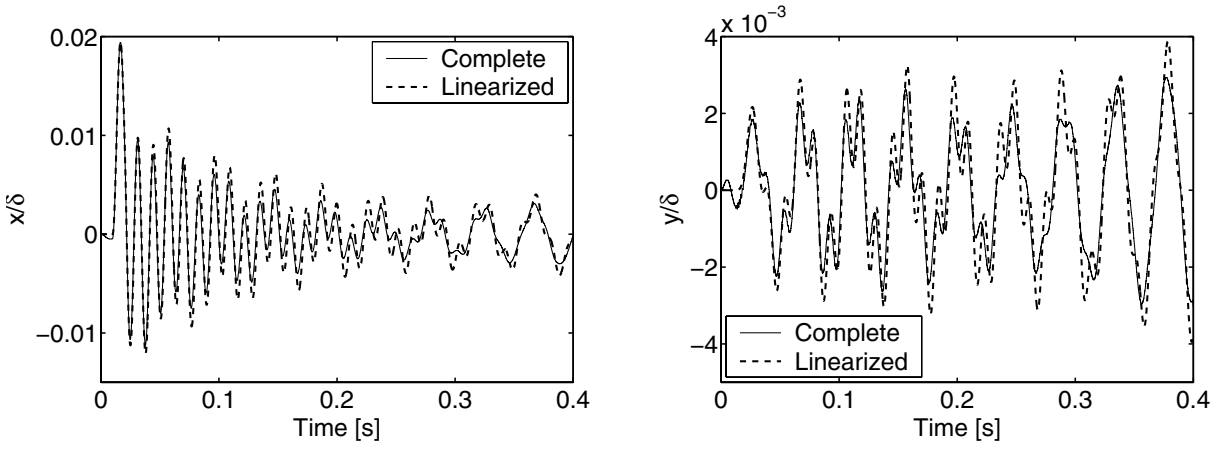

Figure 4: The horizontal (on the left) and vertical (on the right) displacement response obtained by the complete and linearized simulation models. The displacements are related to the air gap length, $\delta = 0.45\,\text{mm}$. The excitation force, $F = 30\,\text{N}$, was exerted on the rotor in the horizontal direction between $t_1 = 0.01\,\text{s}$ and $t_2 = 0.02\,\text{s}$. The first cut-off frequency of this excitation is 100 Hz.

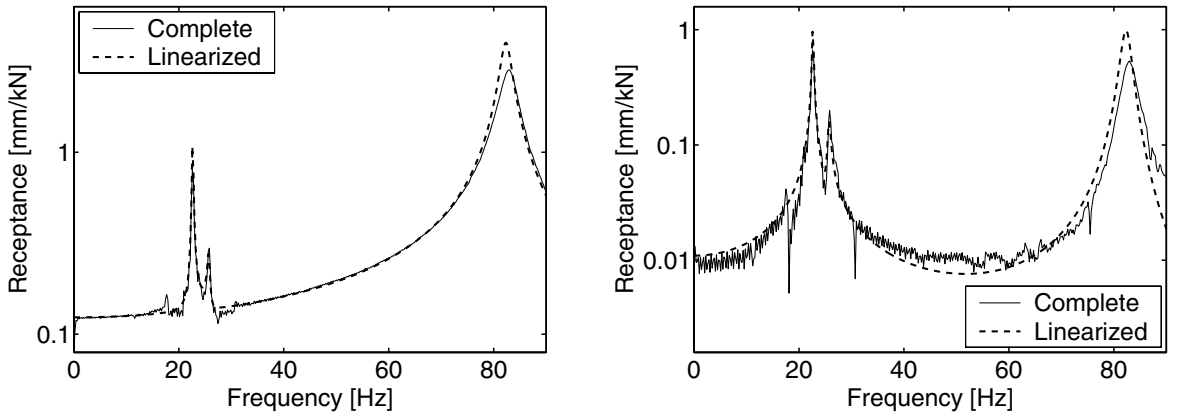

Figure 5: The frequency response functions between the horizontal (on the left) and vertical displacements (on the right) and the horizontal excitation. See text for the details.

4 Discussion of the results

Figure 2a represents the solved magnetic field for the whirling rotor. However, only the fundamental field component, which has two pole pairs ($p = 2$), is visible. This is due to the weakness of other field components. The difference field, presented in Figure 2b, reveals the other most important field components of the disturbed magnetic field. The visible harmonic components of this disturbed field are $p-1$ and $p+1$. These field components are known to be the two most important harmonic components related to the generation of electromagnetic total force at the low frequency range [1, 4]. In addition, it can be observed that the maximum value of the magnetic field induced by the whirling motion is about 2 % of the maximum value of the fundamental field. This indicates that the numerical accuracy required for the electromagnetic field calculations in electromechanical problems is high.

The relation between the rotordynamic stability and the shaft stiffness can be seen in Figure 3. Only the results of the complete model are represented. The linearized model gave similar orbits. The addition of the non-rotating mechanical damping enhanced stability. However, the main characteristics of the system remained qualitatively unchanged.

Figure 4 shows the transient responses for an impulse excitation. The complete and linearized simulation models yield mainly similar responses. However, the higher frequency components attenuate faster in the complete model. The higher frequency components, corresponding to the mechanical vibrations, dominate in the beginning of the horizontal response. This initial phase is followed by the domination of a lower frequency component, which is related to one of the electromagnetic eigenmodes. The unstable behavior follows, though, it is not observable in Figure 4. It can also be observed, as well as in Figure 3, that the horizontal and vertical directions are coupled via the electromechanical interaction.

Figure 5 shows that the frequency response functions of the simulation and parametric model are very similar. Two of the eigenfrequencies (22.6 Hz and 25.8 Hz) are related to the harmonic components $p-1$ and $p+1$ of the electromagnetic field. The third eigenfrequency (83 Hz) is related to the mechanical eigenmode, which is coupled with the electromagnetic system. The calculated curves differ especially around the third eigenfrequency. A potential explanation for this discrepancy between the models is the estimation procedure for the electromagnetic force parameters. These parameters for the linearized model were obtained by curve fitting procedure using the frequency range 0 – 50 Hz weighting the frequency range close to the electromagnetic resonances at about 24 Hz (Figure 1). This means that the electromagnetic forces around the mechanical eigenfrequency (83 Hz) are extrapolated far away from the original data values. This extrapolation error is included in the linearized model, but not in the complete model. A cross-check of the parametric force model together with the simulated force values at higher frequencies confirm that this hypothesis explains, at least, part of the discrepancy.

5 Conclusions

The numerical results indicate that the linearized simulation model can be used as a good approximation, when the effects of electromechanical interaction in rotor vibrations of electric machines are investigated. In this linearized model, the parametric force model represents the electromagnetic forces between the rotor and stator. This force model is linear in respect to the rotor position. The use of this linearized model is very attractive, especially in practical applications, because it is computationally very effective.

An important observation is related to the estimation procedure of the electromagnetic force parameters. In the estimation procedure, which was in this study the curve fitting technique, the frequency range of the investigated phenomena must be taken into account. To enhance the quality of

the model on the critical frequency ranges, it is attractive to use a weighting function or introduce a few additional force parameters.

The mechanical model of the coupled electromechanical system was very simple even in the complete simulation model. The obtained results encourage, in the future, to couple more detailed mechanical models together with the electromagnetic models of electric machines.

Acknowledgements

The authors gratefully acknowledge the financial support of the National Technology Agency of Finland (Tekes). Special thanks are due to Dr. Seppo Aatola, VTT Industrial Systems, for valuable advice concerning the spectral analysis techniques.

References

[1] J. Früchtenicht, H. Jordan, H. O. Seinsch, *Exzentrizitätsfelder als Ursache von Laufinstabilitäten bei Asynchronmaschinen*, Arch. für Electrotechnik, 65, (1982), 271–292.

[2] R. Belmans, A. Vandenput, W. Geysen, *Calculation of the flux density and the unbalanced pull in two pole induction machines*. Arch. für Electrotechnik, 70, (1987), 151–161.

[3] D. Skubov, I. V. Shumakovich, *Stability of the rotor of an induction motor in the magnetic field of the current windings*, Mechanics of solids, 34(4), (1999), 28–40. (Translated from Mekhanika Tverdogo Tela, 4, 36–50, 1999)

[4] A. Arkkio, M. Antila, K.Pokki, A. Simon, E. Lantto, *Electromagnetic force on a whirling cage rotor*, IEEE Proc. – Electr. Power Applications, 147, (2000), 353–360.

[5] T. P. Holopainen, A. Tenhunen, A. Arkkio, *Electromagnetic circulatory forces and rotordynamic instability in electric machines*, in *Rotor Dynamics. Proc. 6th Int. Conf., Sydney*, *2002*, submitted to review process.

[6] A. Arkkio, *Analysis of induction motors based on the numerical solution of the magnetic field and circuit equations*, Acta Polytechnica Scandinavia, Electrical Engineering Series, 59, (1987).

[7] J. L. Coulomb, *A methodology for the determination of global electromechanical quantities from a finite element analysis and its application to the evaluation of magnetic forces*, torques and stiffness. IEEE Transactions on Magnetics, 19, (1983), 2514–2519.

[8] D. J. Ewins, *Modal testing: theory, practice and application*, 2nd ed., Research Studies Press Ltd., Hertfordshire, England (2000).

[9] Anon., *MATLAB Manuals (version 5.3.1)*, The MathWorks, Inc., Natick, Massachusetts (2001). http://www.mathworks.com